

# Topological magnons in a non-coplanar magnetic order on the triangular lattice

Linli Bai<sup>1,2</sup>, Ken Chen<sup>1,2,\*</sup>

<sup>1</sup> School of Physical Science and Technology & Key Laboratory for Magnetism and Magnetic Materials of the MoE, Lanzhou University, Lanzhou 730000, China.

<sup>2</sup> Lanzhou Center for Theoretical Physics, Key Laboratory of Theoretical Physics of Gansu Province, and Key Laboratory of Quantum Theory and Applications of MoE, Lanzhou University, Lanzhou, Gansu 730000, China.

\*chenk20@lzu.edu.cn

## Abstract

The bond-dependent Kitaev interaction  $K$  is familiar in the effective spin model of transition metal compounds with octahedral ligands. In this work, we find a peculiar non-coplanar magnetic order can be formed with the help of  $K$  and next nearest neighbor Heisenberg coupling  $J_2$  on triangular lattice. It can be seen as a miniature version of skyrmion lattice, since it has nine spins and integer topological number in a magnetic unit cell. The magnon excitations in such an order is studied by the linear spin-wave theory. Of note is that the change in the relative size of  $J_2$  and  $K$  will produce topological magnon phase transitions although the topological number remains unchanged. We also calculated the experimentally observable thermal Hall conductivity, and found that the signs of thermal Hall conductivity will change with topological phase transitions or temperature changes in certain regions.

Keywords: non-coplanar magnetic order; topological magnons; thermal Hall effect.

## 1 Introduction

Magnon is the quanta of the low energy collective excitation in magnetic system [1–3]. Since magnon travels will not produce Joule heating and have much longer diffusion length than electron [4–6], it have application prospects of storing and disseminating information in future [6]. Inspired by topological insulators which can support chiral edge/surface states that are immune to backscattering [7,8], researchers are also committed to finding corresponding objects in magnon [9–16]. Topological non-trivial magnon can be driven by thermal gradient, forming transverse heat current by the Berry phase mechanism [17]. This is called the thermal Hall effect (THC) [18–30]. THC has been experimentally observed in pyrochlore [19, 21] and kagome [11, 25] ferromagnets, the relevant research is in full swing [27, 31].

The non-planar spin textures with non-zero topological number is also a research focus of condensed matter physics [32–38], and the most representative one is Skyrmion [32, 33]. In the continuous limit, the Skyrmions are topologically protected, which means they cannot be generated or removed by any continuous operation [33]. In the actual magnetic system, although the lattice is discrete and the size of the Skyrmions is limited, skyrmion is still relatively stable, which allows it to be manipulated independently as a quasi-particle [39]. In recent years, researchers began to pay attention to the magnon excitations in the Skyrmion [6]. The topological magnon in ferromagnetic and anti-ferromagnetic skyrmion lattices (SkXs) has been discovered [40–46], and the topological phase transitions caused by the interactions or magnetic field are discussed as well [42, 43]. However, as far as we know, in previous work, researchers mainly involved the Skyrmion in non-centrosymmetric magnets which is formed with the help of chiral Dzyaloshinskii-Moriya interaction. This is just the tip of the iceberg of topological non-trivial spin textures [37]. On the one hand, it has been proved that skyrmion can also appear in the centrosymmetric magnets with the help of other interactions [47–58], such as dipolar interaction [47, 54], the single-ion anisotropy [48–53, 55, 56] or the bond-dependent interactions [51, 59]. On the other hand, beyond skyrmion, there are many magnetic quasi-particles

coming into the sight of researchers in recent years [37, 60, 61]. Whether there is topological magnon or even relevant phase transition exist in such spin textures are need for further exploration.

In this work, we study the interplay of Heisenberg and Kitaev interactions on the triangular lattice. The bond-dependent Kitaev interaction are widely considered in the theoretical model describing transition metal compounds with octahedra crystal field [62–64]. We find a peculiar non-coplanar magnetic order can be formed by the competition between  $K$  and next nearest neighbor Heisenberg coupling  $J_2$ . There are nine spins in a magnetic unit cell and the topological number is  $\pm 1(\pm 2)$ , thus it can be seen as a miniature version of (high-Q) SkX [65]. Then we focus on the magnon excitations in such order. Through the linear spin-wave theory, we calculate the Chern number of each magnon band, and based on this, different regions were distinguished. The change of  $J_2$  will produce topological phase transitions although the topological number in real space remains unchanged. Since thermal Hall conductivity is related to the magnon band topology [29], finally, we calculated the thermal Hall conductivity and discussed its distinctions in different areas. Thermal Hall conductivity is dominated by the Berry curvature in the lowest bands at low temperatures. We also found that in certain regions, the signs of thermal Hall conductivity will change with topological phase transitions or temperature changes.

## 2 Model

We consider the following model on triangular lattice,

$$\mathcal{H} = J_2 \sum_{\langle\langle ij \rangle\rangle} \mathbf{S}_i \cdot \mathbf{S}_j + K \sum_{\langle ij \rangle_\gamma} S_i^\gamma S_j^\gamma - \mathbf{h} \cdot \sum_i \mathbf{S}_i \quad (1)$$

where  $J_2$  is the exchange parameters of the second-nearest neighbor Heisenberg coupling, respectively.  $S_i$  represents the spin at site  $i$  and  $S_i^\gamma = \mathbf{S}_i \cdot \vec{\gamma}$ ,  $\vec{\gamma} = \mathbf{x}, \mathbf{y}, \mathbf{z}$  are bond-dependent orthogonal Ising axes. Thus,  $K$  is exchange parameter of anisotropic Kitaev interaction. The last term is the Zeeman term caused by a magnetic field  $\mathbf{h} = h\mathbf{c}$ , which is out of plane. The global coordinate System is shown in Fig. 1 (a), wherein  $\mathbf{c}$  is perpendicular to the triangular plane. Since the Kitaev interaction appears along with octahedral ligands in actual materials [64], the relationship between the  $\mathbf{x}$ - $\mathbf{y}$ - $\mathbf{z}$  and the  $\mathbf{a}$ - $\mathbf{b}$ - $\mathbf{c}$  coordinates systems satisfies

$$\begin{pmatrix} S_x \\ S_y \\ S_z \end{pmatrix} = \begin{pmatrix} \frac{1}{\sqrt{2}} & \frac{1}{\sqrt{6}} & \frac{1}{\sqrt{3}} \\ -\frac{1}{\sqrt{2}} & \frac{1}{\sqrt{6}} & \frac{1}{\sqrt{3}} \\ 0 & -\frac{2}{\sqrt{6}} & \frac{1}{\sqrt{3}} \end{pmatrix} \begin{pmatrix} S_a \\ S_b \\ S_c \end{pmatrix}. \quad (2)$$

We implement the parallel-tempering Monte Carlo simulations [66, 67] to uncover the spin textures. After Monte Carlo simulations, the classic ground state is then obtained by iteratively aligning the spins with their local fields [68]. Other numerical energy optimization methods are also used to check if the energy is at a minimum. Then we use the ground-state energy as well as the spin structure factor  $\mathcal{S}_{\mathbf{k}} = \frac{1}{N_{total}} |\sum_i \mathbf{S}_i e^{-i\mathbf{k} \cdot \mathbf{R}_i}|^2$  [47, 69] to distinguish different phases. In the following, all the spin configurations are plotted in the  $\mathbf{a}$ - $\mathbf{b}$ - $\mathbf{c}$  coordinate system.

## 3 The non-coplanar order

Through the above methods, we find a non-coplanar order can be stabled by the competition between negative  $K$  and small positive  $J_2$ . We take a representative point ( $K = -1$ ,  $J_2 = 1$ ,  $h = 0.05$ ) as an example to illustrate its typical spin configuration in Fig.1 (a), it has  $C_3$  rotational symmetry around the  $\mathbf{c}$ -axis. There are nine spins in a magnetic unit cell  $N = 9$  and the ordering wave vector locates at  $2\mathbf{M}/3$  point, see Fig.1 (b). Since skyrmion has integer topological number in a magnetic unit cell, first, we calculate the solid angle  $\Omega_\Delta$  of each elementary triangle. In the discrete lattice, it can be obtained as [70]

$$\cos\left(\frac{\Omega_\Delta}{2}\right) = \frac{1 + \mathbf{S}_i \cdot \mathbf{S}_j + \mathbf{S}_i \cdot \mathbf{S}_k + \mathbf{S}_j \cdot \mathbf{S}_k}{\sqrt{2(1 + \mathbf{S}_i \mathbf{S}_j)(1 + \mathbf{S}_i \mathbf{S}_k)(1 + \mathbf{S}_j \mathbf{S}_k)}}, \quad (3)$$

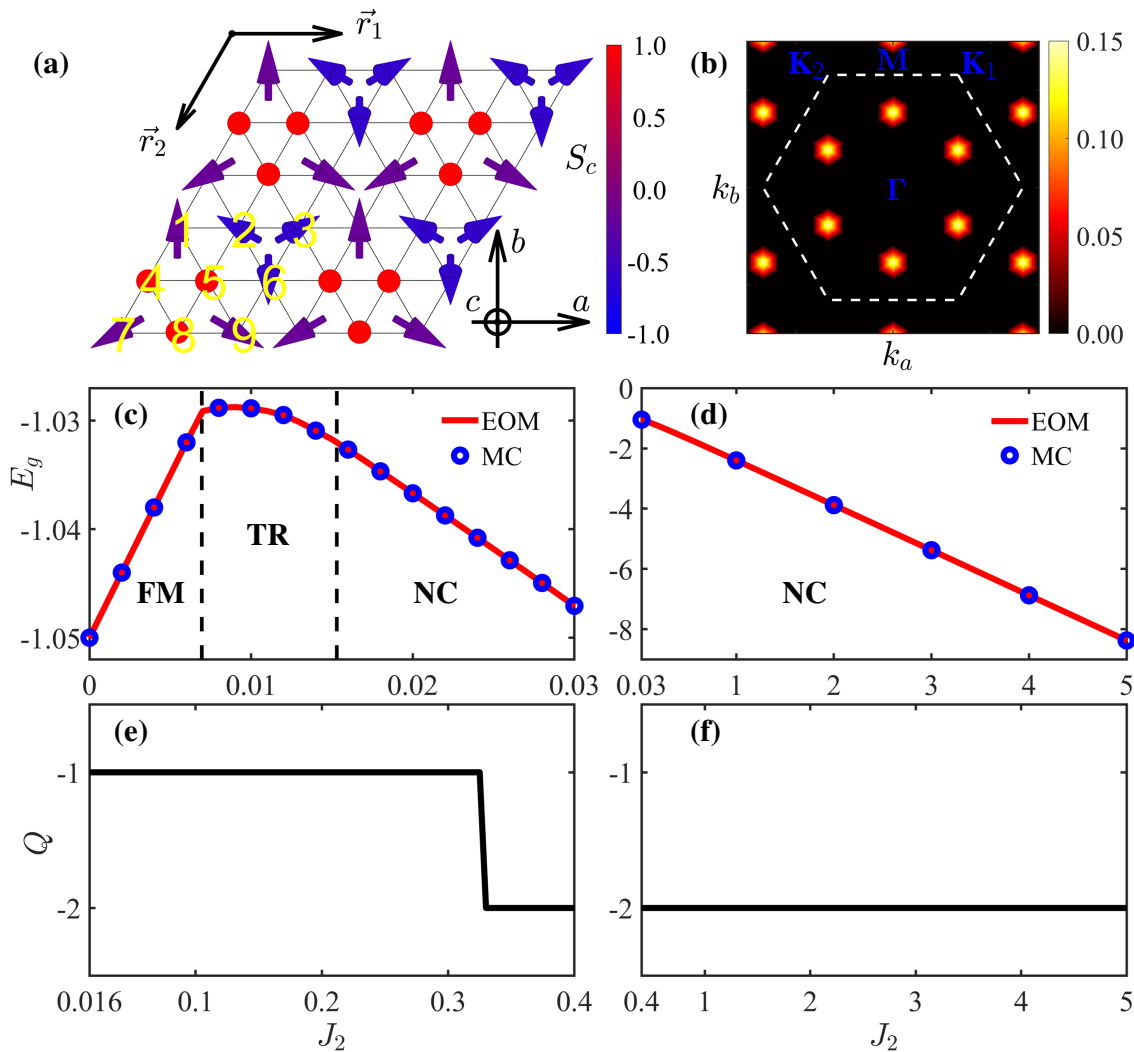


Figure 1: (a) Typical spin configuration of the non-coplanar order when  $K = -1$ ,  $J_2 = 1$ , and  $h = 0.05$ . The small arrows indicate directions of spins and their colors are based on the out of plane component. The magnetic unit cell includes nine spins  $N = 9$ . (b) The spin structure factor corresponds with (a), the peaks locate at  $2\mathbf{M}/3$  point. (c)-(d) The classic energy as a function of  $J_2$  when  $K = -1$ ,  $h = 0.05$ . The result of energy optimization method (EOM) and Monte Carlo method are consistent. The ground state starts from the ferromagnetic (FM) order and rapidly transitions through a narrow transition region (TR) to the non-coplanar (NC) order. As  $J_2$  increases further, the ground state remains in non-coplanar order. (e)-(f) The topological number  $Q$  versus  $J_2$  in the non-coplanar order region. The topological number changes from  $-1$  to  $-2$  when  $J_2 \approx 0.326$ .

where  $\mathbf{S}_i$  is the spin at site  $i$ . The sign of  $\Omega_\Delta$  is determined as  $\text{sign}(\Omega_\Delta) = \text{sign}[\mathbf{S}_i \cdot (\mathbf{S}_j \times \mathbf{S}_k)]$ . Note that on each triangle, the  $i$ ,  $j$ , and  $k$  are arranged counterclockwise. The topological number  $Q$  is the sum of solid angles in a magnetic unit cell,

$$Q = \frac{1}{4\pi} \sum_{\Delta} \Omega_{\Delta} \quad (4)$$

The topological number  $Q$  of the non-coplanar order can be  $\pm 1$  or  $\pm 2$  (for detail, see the next paragraph), and the positive and negative signs can be selected by magnetic fields of different signs. The magnetic field is not the cause of the formation of this magnetic order, but it can eliminate the degeneracy when all spins are reversed.

Now we illustrate the influence of  $J_2$  interaction. The ground state of the pure Kitaev model is ferromagnetic order [71]. As shown in Fig. 1(c), after fixing  $K = -1$  and  $h = 0.05$ , a small  $J_2$  ( $\approx 0.016$ ) will induce the non-coplanar order. A narrow transition area has been identified before

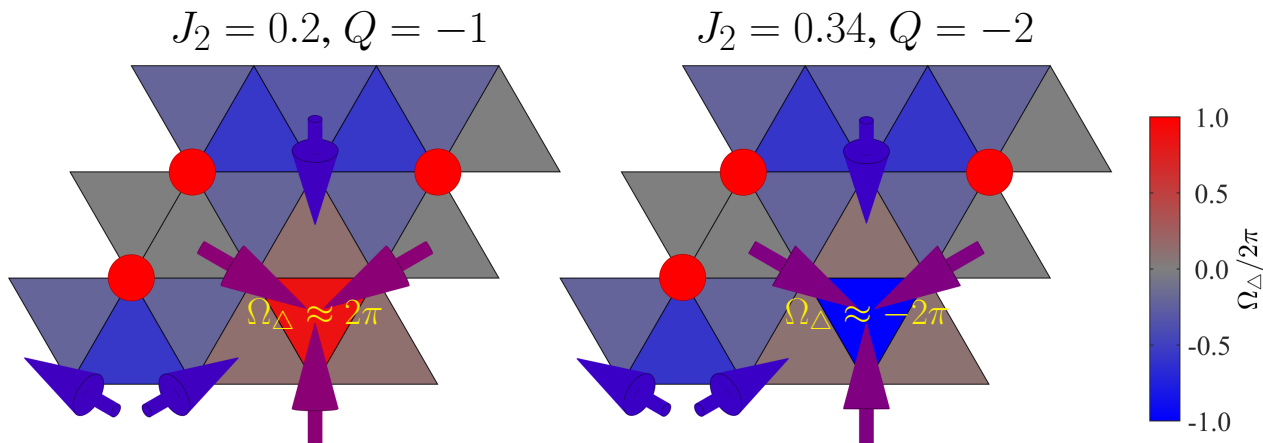


Figure 2: We compared the solid angle  $\Omega_{\Delta}$  distribution when topological number is -1 and -2. Three spins are almost in-plane and they have the same out of plane component  $S_c$ . As  $J_2$  increases, the  $S_c$  continuously changes from a small positive value to a small negative value, the solid angle formed by three spins changes as ( $< 2\pi$ )  $\rightarrow 2\pi \rightarrow -2\pi \rightarrow (> -2\pi)$ . Thus, the topological number (in unit of  $4\pi$ ) as the sum of solid angle reduce by 1.

entering the non-coplanar order, and we omit its details. Then, we continue to increase  $J_2$ , as shown in Fig. 1(d), at least  $J_2$  is less than 5, the non-coplanar order has always existed as the ground state. Of note is that the topological number will undergo a change as  $J_2$  increases. As shown in Fig. 1(e) and (f), when  $J_2 \in [0.016, 0.326]$  the topological number is  $-1$ , and the topological number become  $-2$  when  $J_2$  is larger than 0.326. Since the energy and its derivatives are continuous at  $J_2 \approx 0.326$ , to understand what changes have occurred, we compared the solid angle distribution before and after such point. As shown in Fig. 2, the jump of topological numbers is due to the continuous variation of three almost in-plane spins. They have the same out of plane components  $S_c$  and as  $S_c$  continuously changes from a small positive value to a small negative value, the solid angle formed by three spins will decrease by  $4\pi$ .

## 4 Topological magnon and thermal Hall effect

To consider magnon excitations in our non-coplanar order, we use the linear spin-wave theory, and its detail can be found in Appendix. A. If a magnon band is independent of the upper and lower energy bands, we can capture its topological properties by calculating the Chern number. The Chern number of the band  $n$  ( $C_n$ ) is defined as the integral of the Berry curvature  $\Omega_{n,\mathbf{k}}$  over the first Brillouin zone (FBZ) of magnetic unit cell

$$C_n = \frac{1}{2\pi} \int_{\text{FBZ}} \Omega_{n,\mathbf{k}} d^2\mathbf{k}, \quad (5)$$

and the Berry curvature can be calculated as [28]

$$\Omega_{n,\mathbf{k}} = -2 \text{Im} \sum_{\substack{m=1 \\ m \neq n}}^{2N} \frac{\left( GT_{\mathbf{k}}^\dagger \partial_a \mathcal{H}_{\mathbf{k}} T_{\mathbf{k}} \right)_{nm} \left( GT_{\mathbf{k}}^\dagger \partial_b \mathcal{H}_{\mathbf{k}} T_{\mathbf{k}} \right)_{mn}}{[(G\mathcal{E}_{\mathbf{k}})_{nn} - (G\mathcal{E}_{\mathbf{k}})_{mm}]^2}, \quad (6)$$

where  $G$ ,  $\mathcal{H}_{\mathbf{k}}$ ,  $T_{\mathbf{k}}$  and  $\mathcal{E}_{\mathbf{k}}$  both are  $2N \times 2N$  matrices, and  $G$  is a diagonal matrix whose first  $N$  diagonal elements are 1, and final  $N$  diagonal elements are  $-1$ . The definitions of rest matrices are shown in Appendix. A.

In this section, we mainly focus on the impact of  $J_2$ , and consider a moderate parameter range  $J_2 \in [0.3, 1.2]$  since there are degeneracy points in the energy band when  $J_2$  is smaller. Fig. 3(a)-(c), show the variation of Chern number with  $J_2$  while fixing  $K = -1$ ,  $h = 0.05$ . The nonzero Chern numbers are widely present within the parameter range, indicating the existence of non-trivial band

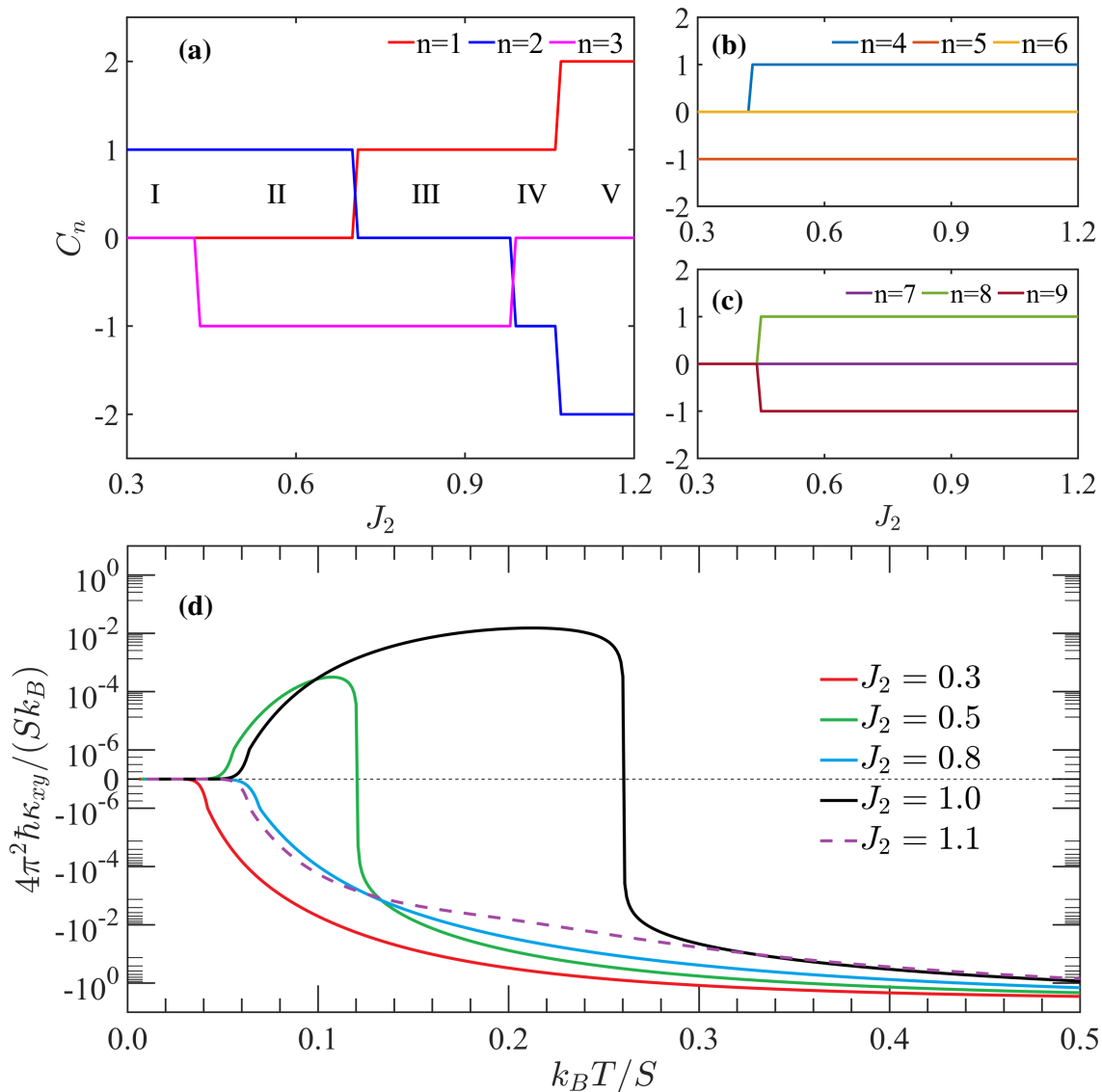


Figure 3: (a)-(c) Chern numbers as a function of  $J_2$ , and  $C_1, C_2, \dots, C_9$  correspond with the lowest to the highest band, respectively. Five areas are distinguished by different Chern numbers. We marked them with Roman numerals I-V in (a). (d) The magnon thermal Hall conductivity as a function of temperature for variant  $J_2$ , which belong to different areas in (a).

topology. The Chern number of the lowest three bands ( $C_1, C_2, C_3$ ) changes with the increase of  $J_2$  as  $(0, 1, 0) \rightarrow (0, 1, -1) \rightarrow (1, 0, -1) \rightarrow (1, -1, 0) \rightarrow (2, -2, 0)$ , sequentially. Five different areas are distinguished, and we marked them with Roman numerals I-V in Fig. 3(a). Specifically, the real space topological number  $Q$  changes from  $-1$  to  $-2$  when  $J_2 \approx 0.326$ , but there is no corresponding topological phase transition occurring at this point. Topological phase transitions mostly occur on the three lowest energy bands, for the rest bands, only  $C_4, C_8$  and  $C_9$  show jumps at  $J_2 \approx 0.43$ . Since magnons follow the Bose-Einstein distribution, they prefer to stay in low energy states at low temperatures, the above fact highlights the importance of the role played by the lower energy bands.

The thermal Hall conductivity (THC) as an observable physical quantity in experiments, is related to the magnon band topology [29]. The THC can be obtained as follows with help of Berry curvature [23],

$$\kappa_{ab} = -\frac{k_B^2 T}{(2\pi)^2 \hbar} \sum_{\mathbf{k} \in \text{FBZ}} \sum_{n=1}^N \left\{ c_2[\rho(E_{n,\mathbf{k}})] - \frac{\pi^2}{3} \right\} \Omega_{n\mathbf{k}}, \quad (7)$$

where  $T$  is temperature,  $N$  is the number of sub-lattices, and  $\rho(E_{n,\mathbf{k}})$  is the Bose distribution function  $\rho(E_{n,\mathbf{k}}) = (e^{E_{n,\mathbf{k}}/k_B T} - 1)^{-1}$ . The weighting function  $c_2(x)$  is defined as  $c_2(x) = (1+x) \ln^2 \frac{1+x}{x} -$

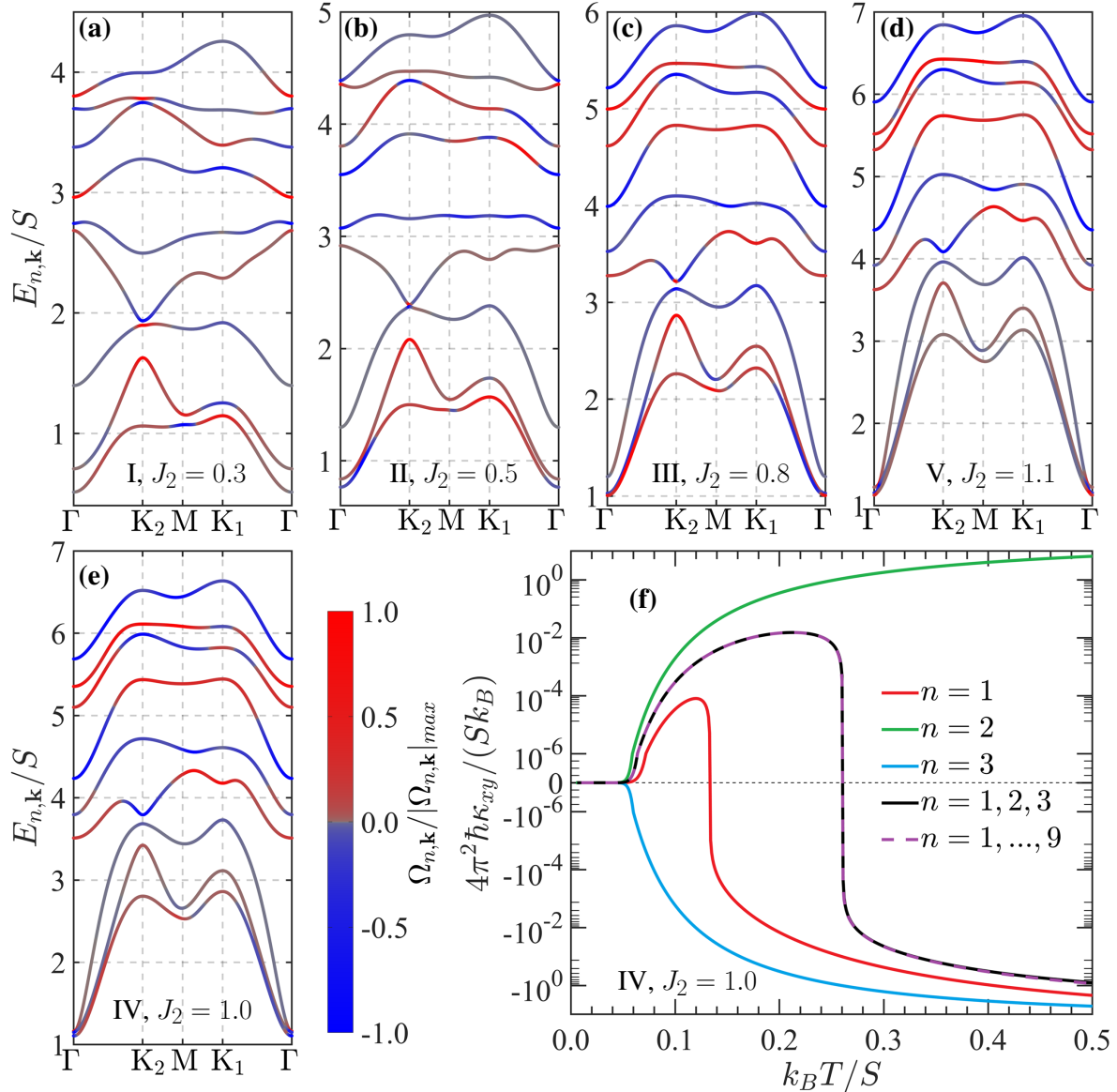


Figure 4: (a-e) Dispersion relations of different values of  $J_2$  when  $K = -1$ ,  $h = 0.05$ . They belong to different areas in Fig. 3(a) respectively. The line color stands for the normalized Berry curvature of each band. (f) The magnon thermal Hall conductivity  $\kappa_{ab}$  as a function of  $k_B T$  at the same parameter point with (e). The curves  $n = 1$ ,  $n = 2$ , and  $n = 3$  are the results coming from the single band  $n$ , and  $n = 1, 2, 3$  is the sum of them.  $n = 1, \dots, 9$  is the overall result which includes nine bands.

$\ln^2 x - 2\text{Li}_2(-x)$  with the Spence function  $\text{Li}_2(z) = -\int_0^z \ln(1-t)/t dt$ .

Fig. 3(d) shows temperature-dependent THC curves of representative points in different areas. At higher temperatures ( $T > 0.34$ ), THC monotonically decreases with increasing  $J_2$ . This relationship no longer exists at low temperatures. Specifically, the curves of  $J_2 = 0.5$  (belongs to area II) and  $J_2 = 1.0$  (belongs to area IV) both show sign change as the temperature changes. Among them, the THC of  $J_2 = 1.0$  has a larger positive area at low temperatures. The curves of rest parameters maintain negative values at low temperatures, and the absolute value of  $J_2 = 0.3$  (belongs to area I) is much larger than that of  $J_2 = 0.8$  ( belongs to area III) and  $J_2 = 1.1$  (belongs to area V).

To further clarify the differences of THC, we present the magnon energy bands with corresponding Berry curvatures of each parameter point in Fig. 4(a)-(e). For all points, the position with the lowest energy is at  $\Gamma$  point. The energy gap at the  $\Gamma$  point indicates the lack of continuous symmetry, and the gap decreases with increasing  $J_2$ . Strictly speaking, all energy bands contribute to THC at finite temperature. However, as the  $c_2$  function drops quickly [10], the THC at low temperature is most related to the Berry curvature in the lowest energy regions. Fig. 4(a) shows the result of  $J_2 = 0.3$ ,

due to the lowest two bands both have positive Berry curvatures near the  $\Gamma$  point, the THC has the maximum negative value at low temperatures. As shown in Fig. 4(b), although the lowest two bands have inverse Berry curvatures near the  $\Gamma$  point when  $J_2 = 0.5$ , the Berry curvatures of the lowest band make greater contributions, resulting totally positive THC at low temperatures. Fig. 4(c) and (d) show the result of  $J_2 = 0.8$  and  $J_2 = 1.1$  respectively. The contribution of Berry curvature to THC near the  $\Gamma$  point has almost been canceled out since Berry curvature has the opposite sign and the lowest two bands are very close.

As shown in Fig. 4(e), the three lowest bands are both close near the  $\Gamma$  point when  $J_2 = 1.0$ . Fig. 4(f) shows the contribution to THC of these bands respectively. It can be seen that the THC of the lowest band  $n = 1$  change sign at  $k_B T/S \approx 0.14$ , this is because the sign of Berry curvature quickly changes from negative to positive outside the  $\Gamma$  point. The second band  $n = 2$  consistently contributes positively to THC, and the contribution of the third band  $n = 3$  to THC is always negative and cannot be ignored at low temperatures. In short, the total negative THC region originates from the combined effect of three bands. Moreover, we also calculated the sum of the lowest three bands, and compared it with the total THC, the two curves are relatively consistent at low temperatures.

## 5 Summary

In summary, we found a peculiar non-coplanar order formed by the competition between bond-dependent Kitaev interaction  $K$  and next nearest neighbor Heisenberg coupling  $J_2$  in triangular lattice. It can be seen as a miniature version of (high-Q) SkX since its magnetic unit cell includes nine spins and has the  $\pm 1(\pm 2)$  topological number. Through the linear spin-wave theory, we studied the magnon excitations in such order, the dispersions and the corresponding Chern numbers is obtained as well. Multiple topological phases (areas) are distinguished by the Chern numbers. Of note is that the change in the relative size of  $J_2$  and  $K$  will produce topological phase transitions although the topological number in real space remains unchanged. Then we calculated the thermal Hall conductivity and discussed its differences in different areas. We found that the thermal Hall conductivity is dominated by the Berry curvature in the lowest bands at low temperatures, and in certain regions, the signs of thermal Hall conductivity will change with topological phase transitions or temperature changes. Based on these results, we hope our work will enlighten the future research of magnonics on trigonal Kitaev materials.

## Acknowledgments

We thank Rui-bo Wang for useful feedback on the manuscript. This research was supported in part by Supercomputing Center of Lanzhou University.

## A Linear spin wave theory

When considering the magnon excitations in a non-coplanar configuration with multiple spins in a magnetic unit cell, we perform the Holstein-Primakoff (HP) transformation with the quantization axis based on spin orientation. In our global coordinate system, the orientation of spin  $i$  is

$$\mathbf{S}_i = \left( S_i^a, S_i^b, S_i^c \right) = (\sin \theta_i \cos \phi_i, \sin \theta_i \sin \phi_i, \cos \theta_i). \quad (8)$$

With the help of polar angles, we can find a rotation matrix

$$R_i = \begin{bmatrix} \cos \theta_i \cos \phi_i & -\sin \phi_i & \sin \theta_i \cos \phi_i \\ \cos \theta_i \sin \phi_i & \cos \phi_i & \sin \theta_i \sin \phi_i \\ -\sin \theta_i & 0 & \cos \theta_i \end{bmatrix}, \quad (9)$$

and determine a local coordinate system  $\tilde{\mathbf{a}}\tilde{\mathbf{b}}\tilde{\mathbf{c}}$  that satisfying  $(S_i^a, S_i^b, S_i^c)^T = R_i (S_i^{\tilde{a}}, S_i^{\tilde{b}}, S_i^{\tilde{c}})^T$ . The spin model Eq.[1] can be rewritten as

$$\mathcal{H} = \sum_{\langle i,j \rangle, \langle\langle i,j \rangle\rangle} \mathbf{S}_i^T \cdot J_{ij} \cdot \mathbf{S}_j - \sum_i \mathbf{h} \cdot \mathbf{S}_i, \quad (10)$$

where  $J_2$  and  $K$  terms are uniformly written into the interaction matrix  $J_{ij}$ . After performing coordinate transformation on all spins separately, the model has the following form [72]

$$\mathcal{H} = \sum_{\langle i,j \rangle, \langle\langle i,j \rangle\rangle} \tilde{\mathbf{S}}_i^T R_i^T \cdot R_i \tilde{J}_{ij} R_j^T \cdot R_j \tilde{\mathbf{S}}_j - \sum_i \tilde{\mathbf{h}} R_i^T \cdot R_i \tilde{\mathbf{S}}_i. \quad (11)$$

The Holstein-Primakoff expansion [73] on spin  $i$  is

$$\begin{aligned} S_i^{\tilde{c}} &= S - b_i^\dagger b_i = S - n_i \\ S_i^{\tilde{a}} &= \frac{\sqrt{2S - n_i} b_i + b_i^\dagger \sqrt{2S - n_i}}{2} \approx \sqrt{\frac{S}{2}} (b_i + b_i^\dagger) \\ S_i^{\tilde{b}} &= \frac{\sqrt{2S - n_i} b_i - b_i^\dagger \sqrt{2S - n_i}}{2} \approx -i \sqrt{\frac{S}{2}} (b_i - b_i^\dagger), \end{aligned} \quad (12)$$

and we keep only the lowest order of the boson operator. Then we substitute  $\tilde{\mathbf{S}}_i = \left( S_i^{\tilde{a}}, S_i^{\tilde{b}}, S_i^{\tilde{c}} \right)^T$  for each spin in a magnetic unit cell and apply the Fourier transformation

$$b_i = b_{n,j} = \frac{1}{\sqrt{L}} \sum_{\mathbf{k} \in \text{FBZ}} b_j(\mathbf{k}) e^{i\mathbf{k} \cdot (\mathbf{V}_n + \mathbf{r}_j)}, \quad (13)$$

where  $n$  is index of unit cell,  $j \in (1, \dots, N)$  marks the sub-lattice inside unit cell,  $L$  is the total number of unit cells and  $\mathbf{V}_n$  is Bravais lattice coordinate. Finally, we can obtain the spin wave Hamiltonian, and we focus on the quadratic term,

$$\mathcal{H}_2 = \frac{1}{2} \sum_{\mathbf{k}} \psi_{\mathbf{k}}^\dagger \mathcal{H}_{\mathbf{k}} \psi_{\mathbf{k}} \quad (14)$$

where  $\psi_{\mathbf{k}}^\dagger = \left( a_{1,\mathbf{k}}^\dagger, a_{2,\mathbf{k}}^\dagger, \dots, a_{N,\mathbf{k}}^\dagger, a_{1,-\mathbf{k}}, a_{2,-\mathbf{k}}, \dots, a_{N,-\mathbf{k}} \right)$  and  $\mathcal{H}_{\mathbf{k}}$  is a  $2N \times 2N$  matrix. We can use a transformation matrix  $T_{\mathbf{k}}$  to diagonalize the matrix  $\mathcal{H}_{\mathbf{k}}$  [74],

$$\mathcal{E}_{\mathbf{k}} = T_{\mathbf{k}}^\dagger \mathcal{H}_{\mathbf{k}} T_{\mathbf{k}}, \quad (15)$$

where  $\mathcal{E}_{\mathbf{k}} = \text{diag} (E_{1,\mathbf{k}}, E_{2,\mathbf{k}}, \dots, E_{N,\mathbf{k}}, E_{1,-\mathbf{k}}, E_{2,-\mathbf{k}}, \dots, E_{N,-\mathbf{k}})$  contains the magnon dispersions.

## References

- [1] F. Bloch. Zur theorie des ferromagnetismus. *Zeitschrift für Physik*, 61(3):206–219, Mar 1930.
- [2] Ryogo Kubo. The spin-wave theory of antiferromagnetics. *Phys. Rev.*, 87:568–580, Aug 1952.
- [3] Freeman J. Dyson. General theory of spin-wave interactions. *Phys. Rev.*, 102:1217–1230, Jun 1956.
- [4] V V Kruglyak, S O Demokritov, and D Grundler. Magnonics. *Journal of Physics D: Applied Physics*, 43(26):264001, jun 2010.
- [5] A. V. Chumak, V. I. Vasyuchka, A. A. Serga, and B. Hillebrands. Magnon spintronics. *Nature Physics*, 11(6):453–461, Jun 2015.
- [6] Z.-X. Li, Yunshan Cao, and Peng Yan. Topological insulators and semimetals in classical magnetic systems. *Physics Reports*, 915:1–64, 2021.
- [7] M. Z. Hasan and C. L. Kane. Colloquium: Topological insulators. *Rev. Mod. Phys.*, 82:3045–3067, Nov 2010.
- [8] Xiao-Liang Qi and Shou-Cheng Zhang. Topological insulators and superconductors. *Rev. Mod. Phys.*, 83:1057–1110, Oct 2011.



- [9] Lifa Zhang, Jie Ren, Jian-Sheng Wang, and Baowen Li. Topological magnon insulator in insulating ferromagnet. *Phys. Rev. B*, 87:144101, Apr 2013.
- [10] Alexander Mook, Jürgen Henk, and Ingrid Mertig. Magnon hall effect and topology in kagome lattices: A theoretical investigation. *Phys. Rev. B*, 89:134409, Apr 2014.
- [11] R. Chisnell, J. S. Helton, D. E. Freedman, D. K. Singh, R. I. Bewley, D. G. Nocera, and Y. S. Lee. Topological magnon bands in a kagome lattice ferromagnet. *Phys. Rev. Lett.*, 115:147201, Sep 2015.
- [12] Kouki Nakata, Se Kwon Kim, Jelena Klinovaja, and Daniel Loss. Magnonic topological insulators in antiferromagnets. *Phys. Rev. B*, 96:224414, Dec 2017.
- [13] Bo Li and Alexey A. Kovalev. Chiral topological insulator of magnons. *Phys. Rev. B*, 97:174413, May 2018.
- [14] P. A. McClarty, X.-Y. Dong, M. Gohlke, J. G. Rau, F. Pollmann, R. Moessner, and K. Penc. Topological magnons in kitaev magnets at high fields. *Phys. Rev. B*, 98:060404, Aug 2018.
- [15] Zhengwei Cai, Song Bao, Zhao-Long Gu, Yi-Peng Gao, Zhen Ma, Yanyan Shangguan, Wenda Si, Zhao-Yang Dong, Wei Wang, Yizhang Wu, Dongjing Lin, Jinghui Wang, Kejing Ran, Shichao Li, Devashibhai Adroja, Xiaoxiang Xi, Shun-Li Yu, Xiaoshan Wu, Jian-Xin Li, and Jinsheng Wen. Topological magnon insulator spin excitations in the two-dimensional ferromagnet  $\text{CrBr}_3$ . *Phys. Rev. B*, 104:L020402, Jul 2021.
- [16] Paul A. McClarty. Topological magnons: A review. *Annual Review of Condensed Matter Physics*, 13(1):171–190, 2022.
- [17] Ryo Matsumoto and Shuichi Murakami. Theoretical prediction of a rotating magnon wave packet in ferromagnets. *Phys. Rev. Lett.*, 106:197202, May 2011.
- [18] Hosho Katsura, Naoto Nagaosa, and Patrick A. Lee. Theory of the thermal hall effect in quantum magnets. *Phys. Rev. Lett.*, 104:066403, Feb 2010.
- [19] Y. Onose, T. Ideue, H. Katsura, Y. Shiomi, N. Nagaosa, and Y. Tokura. Observation of the magnon hall effect. *Science*, 329(5989):297–299, 2010.
- [20] Ryo Matsumoto and Shuichi Murakami. Rotational motion of magnons and the thermal hall effect. *Phys. Rev. B*, 84:184406, Nov 2011.
- [21] T. Ideue, Y. Onose, H. Katsura, Y. Shiomi, S. Ishiwata, N. Nagaosa, and Y. Tokura. Effect of lattice geometry on magnon hall effect in ferromagnetic insulators. *Phys. Rev. B*, 85:134411, Apr 2012.
- [22] Ryuichi Shindou, Ryo Matsumoto, Shuichi Murakami, and Jun-ichiro Ohe. Topological chiral magnonic edge mode in a magnonic crystal. *Phys. Rev. B*, 87:174427, May 2013.
- [23] Ryo Matsumoto, Ryuichi Shindou, and Shuichi Murakami. Thermal hall effect of magnons in magnets with dipolar interaction. *Phys. Rev. B*, 89:054420, Feb 2014.
- [24] Max Hirschberger, Jason W. Krizan, R. J. Cava, and N. P. Ong. Large thermal hall conductivity of neutral spin excitations in a frustrated quantum magnet. *Science*, 348(6230):106–109, 2015.
- [25] Max Hirschberger, Robin Chisnell, Young S. Lee, and N. P. Ong. Thermal hall effect of spin excitations in a kagome magnet. *Phys. Rev. Lett.*, 115:106603, Sep 2015.
- [26] S. A. Owerre. Topological thermal hall effect in frustrated kagome antiferromagnets. *Phys. Rev. B*, 95:014422, Jan 2017.

- [27] Shuichi Murakami and Akihiro Okamoto. Thermal hall effect of magnons. *Journal of the Physical Society of Japan*, 86(1):011010, 2017.
- [28] Alexander Mook, Jürgen Henk, and Ingrid Mertig. Thermal hall effect in noncollinear coplanar insulating antiferromagnets. *Phys. Rev. B*, 99:014427, Jan 2019.
- [29] Robin R. Neumann, Alexander Mook, Jürgen Henk, and Ingrid Mertig. Thermal hall effect of magnons in collinear antiferromagnetic insulators: Signatures of magnetic and topological phase transitions. *Phys. Rev. Lett.*, 128:117201, Mar 2022.
- [30] Fengjun Zhuo, Jian Kang, Aurélien Manchon, and Zhenxiang Cheng. Topological phases in magnonics. *Advanced Physics Research*, n/a(n/a):2300054.
- [31] Xiao-Tian Zhang, Yong Hao Gao, and Gang Chen. Thermal hall effects in quantum magnets, 2023.
- [32] T.H.R. Skyrme. A unified field theory of mesons and baryons. *Nuclear Physics*, 31:556–569, 1962.
- [33] Naoto Nagaosa and Yoshinori Tokura. Topological properties and dynamics of magnetic skyrmions. *Nature Nanotechnology*, 8(12):899–911, Dec 2013.
- [34] Albert Fert, Nicolas Reyren, and Vincent Cros. Magnetic skyrmions: advances in physics and potential applications. *Nature Reviews Materials*, 2(7):17031, Jun 2017.
- [35] Yan Zhou. Magnetic skyrmions: intriguing physics and new spintronic device concepts. *National Science Review*, 6(2):210–212, 10 2018.
- [36] Alexei N. Bogdanov and Christos Panagopoulos. Physical foundations and basic properties of magnetic skyrmions. *Nature Reviews Physics*, 2(9):492–498, Sep 2020.
- [37] Börge Göbel, Ingrid Mertig, and Oleg A. Tretiakov. Beyond skyrmions: Review and perspectives of alternative magnetic quasiparticles. *Physics Reports*, 895:1–28, 2021.
- [38] Tao Yu, Zhaochu Luo, and Gerrit E.W. Bauer. Chirality as generalized spin–orbit interaction in spintronics. *Physics Reports*, 1009:1–115, 2023. Chirality as Generalized Spin-Orbit Interaction in Spintronics.
- [39] Soong-Geun Je, Hee-Sung Han, Se Kwon Kim, Sergio A. Montoya, Weilun Chao, Ik-Sun Hong, Eric E. Fullerton, Ki-Suk Lee, Kyung-Jin Lee, Mi-Young Im, and Jung-Il Hong. Direct demonstration of topological stability of magnetic skyrmions via topology manipulation. *ACS Nano*, 14(3):3251–3258, Mar 2020.
- [40] A Roldán-Molina, A S Nunez, and J Fernández-Rossier. Topological spin waves in the atomic-scale magnetic skyrmion crystal. *New Journal of Physics*, 18(4):045015, apr 2016.
- [41] Sebastián A. Díaz, Jelena Klinovaja, and Daniel Loss. Topological magnons and edge states in antiferromagnetic skyrmion crystals. *Phys. Rev. Lett.*, 122:187203, May 2019.
- [42] Sebastián A. Díaz, Tomoki Hirose, Jelena Klinovaja, and Daniel Loss. Chiral magnonic edge states in ferromagnetic skyrmion crystals controlled by magnetic fields. *Phys. Rev. Res.*, 2:013231, Feb 2020.
- [43] Kristian Mæland and Asle Sudbø. Quantum topological phase transitions in skyrmion crystals. *Phys. Rev. Res.*, 4:L032025, Aug 2022.
- [44] V. E. Timofeev and D. N. Aristov. Magnon band structure of skyrmion crystals and stereographic projection approach. *Phys. Rev. B*, 105:024422, Jan 2022.

- [45] Masatoshi Akazawa, Hyun-Yong Lee, Hikaru Takeda, Yuri Fujima, Yusuke Tokunaga, Taka-hisa Arima, Jung Hoon Han, and Minoru Yamashita. Topological thermal hall effect of magnons in magnetic skyrmion lattice. *Phys. Rev. Res.*, 4:043085, Nov 2022.
- [46] T. Weber, D. M. Fobes, J. Waizner, P. Steffens, G. S. Tucker, M. Böhm, L. Beddrich, C. Franz, H. Gabold, R. Bewley, D. Voneshen, M. Skoulatos, R. Georgii, G. Ehlers, A. Bauer, C. Pfeiderer, P. Böni, M. Janoschek, and M. Garst. Topological magnon band structure of emergent landau levels in a skyrmion lattice. *Science*, 375(6584):1025–1030, 2022.
- [47] Tsuyoshi Okubo, Sungki Chung, and Hikaru Kawamura. Multiple- $q$  states and the skyrmion lattice of the triangular-lattice heisenberg antiferromagnet under magnetic fields. *Phys. Rev. Lett.*, 108:017206, Jan 2012.
- [48] A. O. Leonov and M. Mostovoy. Multiply periodic states and isolated skyrmions in an anisotropic frustrated magnet. *Nature Communications*, 6(1):8275, Sep 2015.
- [49] Satoru Hayami, Shi-Zeng Lin, and Cristian D. Batista. Bubble and skyrmion crystals in frustrated magnets with easy-axis anisotropy. *Phys. Rev. B*, 93:184413, May 2016.
- [50] Shi-Zeng Lin and Cristian D. Batista. Face centered cubic and hexagonal close packed skyrmion crystals in centrosymmetric magnets. *Phys. Rev. Lett.*, 120:077202, Feb 2018.
- [51] Danila Amoroso, Paolo Barone, and Silvia Picozzi. Spontaneous skyrmionic lattice from anisotropic symmetric exchange in a ni-halide monolayer. *Nature Communications*, 11(1):5784, Nov 2020.
- [52] Satoru Hayami. In-plane magnetic field-induced skyrmion crystal in frustrated magnets with easy-plane anisotropy. *Phys. Rev. B*, 103:224418, Jun 2021.
- [53] Zhentao Wang, Ying Su, Shi-Zeng Lin, and Cristian D. Batista. Meron, skyrmion, and vortex crystals in centrosymmetric tetragonal magnets. *Phys. Rev. B*, 103:104408, Mar 2021.
- [54] Oleg I. Utesov. Thermodynamically stable skyrmion lattice in a tetragonal frustrated antiferromagnet with dipolar interaction. *Phys. Rev. B*, 103:064414, Feb 2021.
- [55] Max Hirschberger, Satoru Hayami, and Yoshinori Tokura. Nanometric skyrmion lattice from anisotropic exchange interactions in a centrosymmetric host. *New Journal of Physics*, 23(2):023039, feb 2021.
- [56] Oleg I. Utesov. Mean-field description of skyrmion lattice in hexagonal frustrated antiferromagnets. *Phys. Rev. B*, 105:054435, Feb 2022.
- [57] Satoru Hayami. Zero-field skyrmion, meron, and vortex crystals in centrosymmetric hexagonal magnets. *Journal of Magnetism and Magnetic Materials*, 564:170036, 2022.
- [58] Satoru Hayami. Anisotropic skyrmion crystal on a centrosymmetric square lattice under an in-plane magnetic field, 2023.
- [59] Xiaoyan Yao and Shuai Dong. Topological triple-vortex lattice stabilized by mixed frustration in expanded honeycomb kitaev-heisenberg model. *Scientific Reports*, 6(1):26750, May 2016.
- [60] Ioannis Rousochatzakis, Ulrich K. Rössler, Jeroen van den Brink, and Maria Daghofer. Kitaev anisotropy induces mesoscopic  $Z_2$  vortex crystals in frustrated hexagonal antiferromagnets. *Phys. Rev. B*, 93:104417, Mar 2016.
- [61] Ken Chen, Qiang Luo, Zongsheng Zhou, Saisai He, Bin Xi, Chenglong Jia, Hong-Gang Luo, and Jize Zhao. Triple-meron crystal in high-spin kitaev magnets. *New Journal of Physics*, 25(2):023006, feb 2023.

- [62] Stephen M Winter, Alexander A Tsirlin, Maria Daghofer, Jeroen van den Brink, Yogesh Singh, Philipp Gegenwart, and Roser Valentí. Models and materials for generalized kitaev magnetism. *Journal of Physics: Condensed Matter*, 29(49):493002, nov 2017.
- [63] Simon Trebst and Ciarán Hickey. Kitaev materials. *Physics Reports*, 950:1–37, 2022.
- [64] Aleksandar Razpopov, David A. S. Kaib, Steffen Backes, Leon Balents, Stephen D. Wilson, Francesco Ferrari, Kira Riedl, and Roser Valentí. A  $j_{eff}=1/2$  Kitaev material on the triangular lattice: the case of NaRuO<sub>2</sub>. *npj Quantum Materials*, 8(1):36, Jul 2023.
- [65] Kazushi Aoyama and Hikaru Kawamura. Emergent skyrmion-based chiral order in zero-field heisenberg antiferromagnets on the breathing kagome lattice. *Phys. Rev. B*, 105:L100407, Mar 2022.
- [66] Koji Hukushima and Koji Nemoto. Exchange monte carlo method and application to spin glass simulations. *Journal of the Physical Society of Japan*, 65(6):1604–1608, June 1996.
- [67] Y Miyatake, M Yamamoto, J J Kim, M Toyonaga, and O Nagai. On the implementation of the 'heat bath' algorithms for monte carlo simulations of classical heisenberg spin systems. *Journal of Physics C: Solid State Physics*, 19(14):2539, may 1986.
- [68] Lukas Janssen, Eric C. Andrade, and Matthias Vojta. Honeycomb-lattice heisenberg-kitaev model in a magnetic field: Spin canting, metamagnetism, and vortex crystals. *Phys. Rev. Lett.*, 117:277202, Dec 2016.
- [69] Tokuro Shimokawa, Tsuyoshi Okubo, and Hikaru Kawamura. Multiple- $q$  states of the  $J_1 - J_2$  classical honeycomb-lattice heisenberg antiferromagnet under a magnetic field. *Phys. Rev. B*, 100:224404, Dec 2019.
- [70] B. Berg and M. Lüscher. Definition and statistical distributions of a topological number in the lattice o(3)  $\sigma$ -model. *Nuclear Physics B*, 190(2):412–424, 1981.
- [71] Michael Becker, Maria Hermanns, Bela Bauer, Markus Garst, and Simon Trebst. Spin-orbit physics of  $j = \frac{1}{2}$  mott insulators on the triangular lattice. *Phys. Rev. B*, 91:155135, Apr 2015.
- [72] Emily Z. Zhang, Li Ern Chern, and Yong Baek Kim. Topological magnons for thermal hall transport in frustrated magnets with bond-dependent interactions. *Phys. Rev. B*, 103:174402, May 2021.
- [73] T. Holstein and H. Primakoff. Field dependence of the intrinsic domain magnetization of a ferromagnet. *Phys. Rev.*, 58:1098–1113, Dec 1940.
- [74] J.H.P. Colpa. Diagonalization of the quadratic boson hamiltonian. *Physica A: Statistical Mechanics and its Applications*, 93(3):327–353, 1978.